Water Research 208 (2022) 117837

Contents lists available at ScienceDirect

Water Research

journal homepage: www.elsevier.com/locate/watres

A model to predict the kinetics of direct (endogenous) virus inactivation by sunlight at different latitudes and seasons, based on the equivalent monochromatic wavelength approach

Ángela García-Gil [a,b], Javier Marugán [a,*], Davide Vione [b,*]

[a] Department of Chemical and Environmental Technology, ESCET, Universidad Rey Juan Carlos, C/ Tulipán s/n, Móstoles, Madrid 28933, Spain
[b] Dipartimento di Chimica, Università di Torino, Via Pietro Giuria 5, Torino 10125, Italy.

ARTICLE INFO

Keywords:
Water disinfection
Solar disinfection
Radiation modeling
Kinetic modeling
Direct photoprocesses

ABSTRACT

Sunlight plays an important role in the inactivation of pathogenic microorganisms such as bacteria and viruses in water. Here we present a model that is able to predict the kinetics of direct virus inactivation (i.e. inactivation triggered by sunlight absorption by the virion, without the role played by photochemically produced reactive intermediates generated by water-dissolved photosensitizers) on a global scale (from 60 °S to 60 °N latitude) and for the different months of the year. The model is based on the equivalent monochromatic wavelength (EMW) approach that was introduced recently, and which largely simplifies complex polychromatic calculations by approximating them with a monochromatic equation at the proper wavelength, the EMW. The EMW equation was initially established for mid-July conditions at a mid-latitude, and was then extended to different seasons and to the latitude belt where the day-night cycle is always observed throughout the year. By so doing, the first-order rate constant of direct virus photoinactivation can be predicted on a global scale, with the use of a relatively simple equation plus tables of pre-calculated input data, as a function of latitude, month, and key water parameters. The model was here applied to the virus organism phiX174, a somatic phage that is often used as proxy for pathogenic viruses undergoing fast direct inactivation, and for which a wide array of published inactivation data is available. Model predictions are validated by comparison with field data of inactivation of somatic phages by sunlight.

1. Introduction

The ability of sunlight to trigger the inactivation of bacteria and viruses occurring in water has been extensively studied in natural water systems (Kohn and Nelson, 2007; Boehm et al., 2009; Love et al., 2010). Furthermore, the same phenomenon has been exploited as a low-cost option to obtain reasonably safe drinking water (solar disinfection or SODIS) (McGuigan et al., 2012), and it may also give a contribution to the treatment of wastewater in waste stabilization ponds and constructed wetlands (Curtis et al., 1994; Silverman et al., 2015). The action of sunlight on microorganisms takes place by two main pathways, of which the first involves direct damage by sunlight photons to (usually) the genome (direct endogenous inactivation) (Nelson et al., 2018). The second pathway requires sunlight absorption by photosensitizers occurring in water, such as chromophoric dissolved organic matter (CDOM), nitrate, and nitrite (Rosado-Lausell et al., 2013; Maraccini et al., 2016). The absorption of sunlight by the photosensitizers triggers the formation of photochemically produced reactive intermediates (PPRIs) such as singlet oxygen ($^1O_2$), hydroxyl radicals ($^\bullet OH$), triplet states of CDOM ($^3CDOM^*$) and carbonate radicals ($CO_3^{\bullet -}$, secondarily formed upon oxidation of HCO_3^- and CO_3^{2-} by $^\bullet OH$, and of CO_3^{2-} by $^3CDOM^*$) (Vione et al., 2014; Rosario-Ortiz and Canonica, 2016; McNeill and Canonica, 2016). These PPRIs can damage viruses and bacteria, and lead to their inactivation (Maraccini et al., 2016; Nelson et al., 2018). Usually, different organisms undergo different inactivation pathways to different extents.

In the case of bacteria there is also a further possibility named indirect endogenous inactivation, where PPRIs are produced within the cell upon absorption of sunlight by photoactive cell constituents (Giannakis et al., 2016). Another difference that can occur between viruses and bacteria is that the former usually show first-order photoinactivation kinetics (Mattle et al., 2015), while the latter can sometimes

* Corresponding authors.
E-mail addresses: javier.marugan@urjc.es (J. Marugán), davide.vione@unito.it (D. Vione).

https://doi.org/10.1016/j.watres.2021.117837
Received 28 July 2021; Received in revised form 10 October 2021; Accepted 1 November 2021
Available online 7 November 2021

repair photodamage at least up to a certain extent. In this case, it may be observed a lag time before the onset of exponential inactivation of bacteria (Giannakis et al., 2018), which considerably complicates the kinetic description of photoinactivation (Serna-Galvis et al., 2019).

As far as the direct (endogenous) photoinactivation is concerned, one important issue is that not all the wavelengths within sunlight have the same effect. Usually, UVB radiation is most effective, followed by UVA and visible. This phenomenon is often described by biological weighting functions or sunlight photoaction spectra, which describe the wavelength-dependent sensitivity to damage by sunlight (Fisher et al., 2011; Nguyen et al., 2014; Silverman et al., 2019). The main reason for the existence of a photoaction spectrum is the fact that absorbance by the genome decreases with increasing wavelength, at least in the range of wavelengths that is relevant to natural sunlight. Based on this consideration, an alternative approach disentangles sunlight absorption by the genome from photon action (Mattle et al., 2015), with a mathematical description that is very similar to the direct photolysis of molecules. This approach has also led to successful modeling of the photoinactivation of viruses (Kohn et al., 2016).

An important difficulty with the modeling of photoinactivation is the polychromatic nature of the phenomenon. This requires quite complex multi-wavelength calculations, and often the use of dedicated software to obtain inactivation kinetics as a function of the environmental conditions (water chemistry, depth, sunlight irradiance, and spectrum) (Zhang et al., 2020). The problem is that software may be seen as a "black box" that is difficult to customize by users, and it is usually not conceived to solve all the problems that may arise in the virus inactivation field.

The same problems occur for the prediction of photodegradation of pollutants by sunlight (Vione, 2020). In the latter context, a recent advance to considerably simplify calculations has been the introduction of the so-called equivalent monochromatic wavelengths or EMW. Following the EMW approach, the polychromatic system is approximated by a much simpler monochromatic equation, and the main issue becomes the identification of the single monochromatic wavelength (the EMW) that ensures the best approximation. Excellent agreement has been observed between the EMW-based monochromatic equation and the multi-wavelength one in the case of organic pollutants (Vione, 2021).

The first goal of this work was to verify whether the EMW approach can be applied successfully to the direct photoinactivation of viruses. We chose viruses instead of bacteria because the behavior of bacteria under sunlight is more complex, and some processes still resist successful modeling (Serna-Galvis et al., 2018). The rationale for choosing direct photoinactivation is that this process is always very significant, and it allows for a single wavelength to be taken into account in calculations when using the EMW approach (*vide infra*). Indeed, even the virus that is most often used as a proxy of indirect (exogenous) inactivation, i.e., the bacteriophage MS2 (Kohn and Nelson, 2007; Kohn et al., 2007; Nelson et al., 2018) is inactivated significantly (around 50% and sometimes even more) by the direct process under a variety of environmental conditions (Kohn et al., 2016). Here, we chose the somatic phage phiX174 as a model virus because this virus undergoes almost exclusively the direct inactivation process (Nelson et al., 2018). Moreover, phiX174 has been studied extensively, and sufficient data are available that allow for successful modeling (Mattle et al., 2015).

The relatively simple form of the EMW equation is amenable to generalizations. Therefore, the second goal of this work was to extend the modeling of virus inactivation (initially carried out for a mid-latitude, mid-July condition) to all seasons and to a wide range of latitudes (60 °S to 60 °N). By so doing, it would be possible to predict the kinetics of virus photoinactivation on the basis of water chemistry and depth, for any season and for a majority of locations on our planet. The added value is that all this would be achieved with a relatively simple and easily manageable equation. Model predictions for the somatic phage phiX174 were then validated against field data that are available for the photoinactivation of somatic phages in natural water, where the direct photoinactivation process is presumed to play a very important role (Bohem et al., 2009). The choice of direct photoinactivation was critical to limit calculations to a single wavelength and to obtain a proof of concept of the feasibility of this approach. The EMW approach can be extended to indirect photoinactivation as well (Vione, 2021), and the global modeling of the indirect processes will be the subject of forthcoming work.

2. Methods

2.1. The EMW approach to virus photoinactivation

To describe the direct photoinactivation of viruses, we used a formalism that is quite similar to that describing the direct photolysis of molecules. Instead of using the so-called photoaction spectrum, this formalism considers the absorption of radiation by the virus and the quantum yield of photoinactivation separately (Mattle et al., 2015). Because of the relatively narrow overlap between virus absorption and sunlight emission (300–320 nm), the photoinactivation quantum yield can be considered constant (Kohn et al., 2016). With this approach, the first-order rate constant of phiX174 photoinactivation is obtained as Eq. (1) in Mattle et al. (2015). By using [L] units for volume, [m] for water depth and referring the solution absorbance to unit dissolved organic carbon (DOC), the mentioned equation in Mattle et al. (2015) takes a form that is similar to the equation describing the direct photolysis of pollutants in Vione (2021):

$$k_{direct} = \frac{10}{d} \int \left[p^o(\lambda) \cdot \Phi \cdot \frac{\varepsilon(\lambda)\,\tau}{A_1(\lambda)\,DOC} \left(1 - 10^{-100\,A_1(\lambda)\;\;d\;\;DOC}\right)\right] d\lambda \qquad (1)$$

where k_{direct} has day^{-1} units, d is the water depth in meters [m], $p^\circ(\lambda)$ [Einstein cm^{-2} s^{-1} nm^{-1}] is a standard sunlight spectral photon flux density (*vide infra*), $\Phi = 1.4 \times 10^{-2}$ mol Einstein^{-1} the quantum yield of phiX174 photoinactivation (Mattle et al., 2015), $\varepsilon(\lambda)$ [M^{-1} cm^{-1}] the molar absorption coefficient of phiX174 (see Fig. 1), τ [s day^{-1}] a conversion factor (*vide infra*), DOC [mg_C L^{-1}] the dissolved organic carbon of the water matrix (natural water or wastewater), and $A_1(\lambda)$ [L mg_C^{-1} cm^{-1}] the absorbance of the water matrix referred to unit DOC and to an optical path length of 1 cm. Note that 100 is the conversion factor between [cm^{-1}] and [m^{-1}], while 10 is the conversion factor between [m^{-1} cm^{-2}] and [L^{-1}]. The total absorbance of the water column is $A_{tot}(\lambda) = A_1(\lambda)\,d\,DOC$, which explains why water depth d appears at the denominator in Eq. (1). This is reasonable because the deeper is

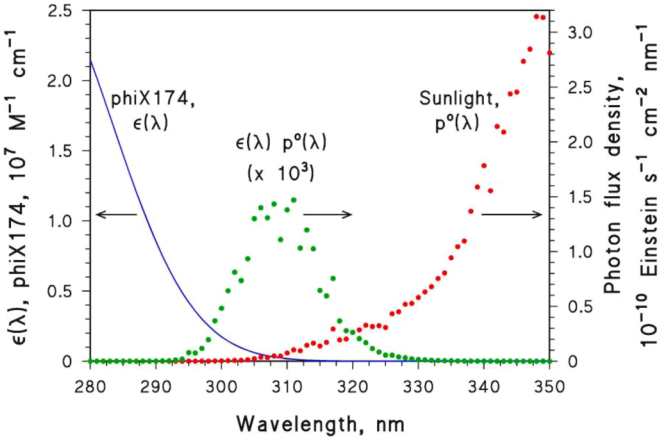

Fig. 1. Left Y-axis: Absorption spectrum $\varepsilon(\lambda)$ (molar absorption coefficient) of the virus phiX174 (Mattle et al., 2015). Right Y-axis: Spectral photon flux density $p^\circ(\lambda)$ of sunlight, equivalent to a UV irradiance of 22 W m^{-2} (Vione, 2020). The product $\varepsilon(\lambda)\,p^\circ(\lambda)$ (units of Einstein L mol^{-1} cm^{-3} s^{-1} nm^{-1}) is also plotted against the right Y-axis.

water, the lower is k_{direct}, and photochemical reactions are slower in deeper waters that are less efficiently illuminated by sunlight (Vione et al., 2014; Kohn et al., 2016).

The chosen standard value of $p^{\circ}(\lambda)$ corresponds to a sunlight UV irradiance (290–400 nm) of 22 W m^{-2} (see Fig. 1), which on a sunny 15 July at 45 °N latitude can be observed at 9 am or 3 pm solar time (solar noon ± 3 h). Of course, such an irradiation condition is not constant during the day, and the conversion factor $\tau = 3.6 \times 10^4$ s day^{-1} takes into account the ratio between constant irradiation at $p^{\circ}(\lambda)$ and actual sunlight intensity from sunrise to sunset (Vione, 2020).

Integration of Eq. (1) is carried out over the wavelength range where absorption by the virus ($\varepsilon(\lambda)$) and sunlight emission ($p^{\circ}(\lambda)$) overlap. With the above data, k_{direct} is obtained as the first-order rate constant of phiX174 photoinactivation on a fair-weather 15 July at 45 °N latitude.

Eq. (1), together with its derivations where $p^{\circ}(\lambda)$ was modified in particular cases (fall equinox) to account for photoinactivation at different latitudes, was found to predict well the behavior of phiX174 under sunlight (Kohn et al., 2016).

It is interesting to observe that Eq. (1) contains all the main parameters that have been shown to affect the photoinactivation of viruses, which is most affected by time and location (which impact $p^{\circ}(\lambda)$), DOC and water depth (Zhang et al., 2020). The current model does not take into account the effects of pH, dissolved oxygen and temperature on virus inactivation. These parameters were found to have limited effect on virus inactivation when varying in the typical ranges found in waste stabilization ponds and constructed wetlands (Maiga et al., 2009; Dias et al., 2017). In contrast, they would play an important role in the framework of the solar disinfection of drinking water (SODIS) (Romero et al., 2011; McGuigan et al., 2012; Carratalà et al., 2016; García-Gil et al., 2020a; Garcia-Gil et al., 2020b). Altitude was also assessed to have limited impact on inactivation (Zhang et al., 2020), most likely because of limited absorption by the virus at or below 300 nm (Fig. 1).

In the case of molecules, it has been shown that the integral calculation based on Eq. (1) can be approximated very well with a much simpler monochromatic equation based on the equivalent monochromatic wavelength (EMW or λ_{eq}) (Vione, 2021). In the case of phiX174, the corresponding monochromatic equation would read as follows:

$$k_{direct} = \frac{10}{d} \cdot p^{\circ}(\lambda_{eq}) \cdot \tau \cdot \eta_{app} \cdot \frac{\varepsilon(\lambda_{eq})}{A_1(\lambda_{eq})\, DOC} \left(1 - 10^{-100\, A_1(\lambda_{eq})\ d\ DOC}\right) \quad (2)$$

where some entries (10, d, τ, DOC, 100) are exactly the same as per Eq. (1), while others ($p^{\circ}(\lambda_{eq})$, $\varepsilon(\lambda_{eq})$, $A_1(\lambda_{eq})$) are referred to the single wavelength λ_{eq} instead of the wavelength range used for integration in Eq. (1). However, the main mechanistic implications (sunlight intensity, virus absorption, water absorption) are the same in both cases and they are thus not lost in Eq. (2) as compared to Eq. (1).

The main difference between the two equations is the replacement of the quantum yield Φ of virus photoinactivation by the apparent photon efficiency η_{app} [nm mol Einstein^{-1}]. $\eta_{app} \gg \Phi$ compensates for the fact that Eq. (2) only considers sunlight absorption by the virus at λ_{eq}, which is much smaller compared to cumulated absorption of radiation over a whole range of wavelengths (Vione, 2021). However, one needs to know Φ for a certain virus in order to derive η_{app}, which means that the mechanistic information contained in Φ cannot be ignored.

To verify whether Eq. (2) with the proper value of λ_{eq} can approximate Eq. (1) well, the following procedure was followed (Vione, 2021):

(i) Use Eq. (1) to produce data of k_{direct} for different values of d and DOC. A good approximation for $A_1(\lambda)$ in several natural water matrices is $A_1(\lambda) = 0.45\ e^{-0.015\ \lambda}$ (Vione, 2020).

(ii) Fit the data thus obtained with Eq. (2). While d, DOC and τ are kept fixed at the same values used for Eq. (1), in a first round $p^{\circ}(\lambda_{eq})$, $\varepsilon(\lambda_{eq})$, $A_1(\lambda_{eq})$ and η_{app} are all defined as free-floating variables. The key value is that of $A_1(\lambda_{eq})$, because it defines the trend of k_{direct} vs. DOC and is not affected by the values of the other variables. Therefore, considering that $A_1(\lambda) = 0.45\ e^{-0.015\ \lambda}$, the value of $A_1(\lambda_{eq})$ obtained by data fit allows for the identification of $\lambda_{eq} = -66.7 \ln [A_1(\lambda_{eq})] - 53.2$ (note that $A_1(\lambda_{eq}) < 1$).

(iii) Once λ_{eq} is obtained, find the corresponding values of $p^{\circ}(\lambda_{eq})$ and $\varepsilon(\lambda_{eq})$ (note that $p^{\circ}(\lambda)$ and $\varepsilon(\lambda)$ are reported in Fig. 1; to aid with similar cases, the corresponding numerical values are also reported in **Table S1** of the Supplementary Material, hereinafter **SM**). At this stage, with fixed $p^{\circ}(\lambda_{eq})$, $\varepsilon(\lambda_{eq})$ and $A_1(\lambda_{eq})$, it is possible to fit the data with η_{app} as the only free-floating variable. If the fit quality is good, it can be concluded that the polychromatic system allows for a convenient EMW approximation.

By using Eq. (2) with fixed values of $p^{\circ}(\lambda_{eq})$, $\varepsilon(\lambda_{eq})$, $A_1(\lambda_{eq})$ and η_{app}, it is possible to predict k_{direct} as a function of d and DOC. These are the most important water parameters as far as direct photoinactivation is concerned (Zhang et al., 2020). Indeed, direct photoprocesses are faster at low d and low DOC, because: *(i)* deep waters are poorly illuminated by sunlight, and *(ii)* high DOC usually means elevated CDOM that competes with the virus for absorption of solar UV radiation.

If Eq. (2) approximates Eq. (1) well, it can be used to predict the value of k_{direct} on 15 July at 45 °N latitude. The given time and latitude depend on the choice of $p^{\circ}(\lambda)$ and τ, which are key issues to generalize the photochemical model to different seasons and latitudes.

2.2. Generalization of the EMW equation

Apart from poorly predictable issues related to the weather, the value of $p^{\circ}(\lambda)$ mostly depends on the time of the day, day of the year and latitude. The problem is that variability is very large and the associated time interval quite short, which may prevent a manageable equation to be obtained. As already done in the case of Eq. (1), a possible way out of the problem is to consider a single spectrum of sunlight that is relevant to the period under consideration, and to match it to the cumulated incident radiation in fair-weather conditions ($G_{day}^{max}(\lambda)$, integral of $p^{\circ}(\lambda)$ over a 1-day time, units of Einstein cm^{-2} day^{-1} nm^{-1}; Kalogirou, 2013). Note that "max" refers to the fact that sunny weather is initially assumed, with different weather conditions lowering the cumulated incident radiation. In the framework of the EMW approximation, $G_{day}^{max}(\lambda)$ becomes the cumulated incident radiation at λ_{eq} ($G_{day}^{max}(\lambda_{eq})$) that can be calculated as follows:

$$G_{day}^{max}(\lambda_{eq}) = \int_{1\ day} p^{o}(\lambda_{eq}, t)\, dt \quad (3)$$

where $p^{\circ}(\lambda_{eq},t)$ takes into account the variability of the spectral photon flux density of sunlight over the time t of the day. The curve of $p^{\circ}(\lambda_{eq},t)$ vs. time that is to be integrated was obtained by using Eqs. (S4,S5) in **SM**, introducing the zenith angles obtained with the Solar Position Algorithm (SPA) from the National Renewable Energy Laboratory (NREL, 2021). The curve was defined with 24 points, i.e., one point for each hour of the day (time step = 3600 s).

As an approximation, $G_{day}^{max}(\lambda_{eq})$ is also given by the product of a single value of $p^{\circ}(\lambda_{eq},t)$, such as the incident spectral photon flux density of sunlight at solar noon ($p_{sn}^{o}(\lambda_{eq})$, units of Einstein cm^{-2} s^{-1} nm^{-1}) times the day length τ_{DL} (the time in [s] from sunrise to sunset), and times a proportionality factor F_1 (unitless). The factor F_1 expresses the relationship between the cumulated incident radiation and the daily dose, if the solar photon flux density corresponds to the solar noon and is constant during the day length (Eq. (4)).

$$G_{day}^{max}(\lambda_{eq}) = F_1 \cdot p_{sn}^{o}(\lambda_{eq}) \cdot \tau_{DL} \quad (4)$$

Detailed procedure to determine the solar photon flux density at solar noon for the equivalent wavelength ($p_{sn}^{o}(\lambda_{eq})$) and the day length τ_{DL} can be found in the **SM**.

Thus, the $G_{day}^{max}(\lambda_{eq})$ data were first computed with Eq. (3) for a latitude of 45 °N, considering the 15th day of each month. These same $G_{day}^{max}(\lambda_{eq})$ data were then optimized with Eq. (4) to obtain the proportionality factor F_1, minimizing the normalized root-mean-square error (NRMSE) between the original data points (Eq. (3)) and those predicted by the fit function (Eq. (4)). Optimization was carried out with Microsoft Excel Solver.

In principle, the value of F_1 obtained for φ = 45 °N might or might not be valid at different latitudes. Therefore, a check was made by computing the values of $G_{day}^{max}(\lambda_{eq})$ with Eq. (3) for the 15th day of each month, at latitudes from 60 °S to 60 °N with steps of 5 °. Then, these data were compared with the predictions obtained with Eq. (4), using $p_{sn}^{o}(\lambda_{eq})$ as per Eq. (S6), τ_{DL} as per Eq. (S7), and the value of F_1 obtained from the previous fit (φ = 45°N).

By replacing the term "$p^{\circ}(\lambda_{eq})\ \tau$" in Eq. (2) with the term "$F_1 \cdot p_{sn}^{o}(\lambda_{eq}) \cdot \tau_{DL}$" as per the above discussion, the first-order rate constants for phiX174 direct photoinactivation are obtained in different months, within the whole latitude belt from 60 °S to 60 °N. This practically includes all of the world's regions where it makes sense to use sunlight to inactivate viruses, as well as the whole continental mainland of the Southern hemisphere (except the Antarctica). The only issue is that this calculated value of k_{direct} refers to fair-weather conditions. A further approach was thus used to take average weather conditions into account. To do so, a new parameter (F_2) was introduced as a cloud-cover factor so that $G_{day}^{real}(\lambda_{eq}) = F_2 \cdot G_{day}^{max}(\lambda_{eq})$ and, therefore:

$$G_{day}^{real}(\lambda_{eq}) = F_2 \cdot F_1 \cdot p_{sn}^{o}(\lambda_{eq}) \cdot \tau_{DL} \quad (5)$$

The value of F_2 is variable even for the same location and day of the year since it depends on the weather conditions. This parameter can be calculated experimentally or estimated using historical data. It is strongly recommended to measure the actual irradiance in the field and calculate F_2 by dividing the experimental value by the theoretical value. However, if actual measurements are not available, F_2 can be estimated using historical data according to the procedure described by Moreno-SanSegundo et al. (2021). This tool calculates the cumulated radiation by applying a cloud-cover factor based on the historical data of the last 12 years with a grid of 0.5° in latitude and longitude. The developed code is openly available at the Github and Zenodo repositories (Moreno-SanSegundo et al., 2021). The values of F_2 as a function of the latitude and longitude geocoordinates are available in the Excel file (F2.xlsx) provided as **SM**.

The value of F_2 allows for modifying Eq. (2) as follows:

$$k_{direct} = \frac{10}{d} \cdot F_2 \cdot F_1 \cdot p_{sn}^{o}(\lambda_{eq}) \cdot \tau_{DL} \cdot \eta_{app} \cdot \frac{\varepsilon(\lambda_{eq})}{A_1(\lambda_{eq}) \cdot DOC} \left(1 - 10^{-100 \cdot A_1(\lambda_{eq}) \cdot d \cdot DOC}\right) \quad (6)$$

Eq. (6) is an estimate of k_{direct} under realistic weather conditions. It should be remarked that all the procedure leading to the elaboration of Eq. (6) was hugely simplified by the possibility to operate at a single wavelength instead of a range of wavelengths. This is enabled by the EMW approach, which also allows for eventually obtaining a relatively simple equation that does not require numerical integration to be solved.

This model was validated in two different ways with literature data. Firstly, the cumulated incident radiation was compared with data of average sunlight spectra, available from 8:00 to 16:00 h solar time at a latitude of 52°N (Frank and Klöpffer, 1988). Briefly, the cumulated incident radiation was obtained following $G_{day}^{real}(\lambda_{eq}) = F_2 \cdot G_{day}^{max}(\lambda_{eq})$. On the one hand, $G_{day}^{max}(\lambda_{eq})$ was calculated with Eq. (3) for the 15th day of each month, carrying out integration over time from 8.00 h to 16.00 h. Again, the $p^{\circ}(\lambda_{eq})$ vs. time curve was obtained using Eqs. (S4, S5) with φ = 52 °N, and by introducing the zenith angles obtained from NREL (2021). The curve was defined with 8 points, i.e., one point per hour (8.00–16.00 h, time step = 3600 s). On the other hand, F_2 was obtained for 52 °N latitude and 5 °E longitude using the Excel file (F2.xlsx) provided as **SM**.

Secondly, Eq. (6) was used to assess published field data of virus photoinactivation. In particular, Boehm et al. (2009) studied the photoinactivation rate constants of somatic phages measured in a lagoon in Avalon Bay, California (20th–23rd August, latitude: 33 °N), and suggested that direct photoinactivation would play an important role. Key water conditions were 15 cm water depth and 7 $mg_C\ L^{-1}$ DOC. The disinfection kinetic constant predicted with our model for direct photoinactivation of the somatic phage phiX174 was compared with the observed disinfection kinetic constant that has been determined as 28 $day^{-1}\ I_{UVB}{}^{-1}$, where I_{UVB} is the irradiance of sunlight in the UVB region (Boehm et al., 2009). The parameter F_2 for Eq. (6) was obtained as usual with the F2.xlsx file provided in the **SM**, for 33 °N latitude and 118 °E longitude.

3. Results and discussion

3.1. EMW approximation of photoinactivation kinetics

The values of k_{direct} for phiX174 as a function of DOC and water depth d were first calculated with Eq. (1), using the values of $p^{\circ}(\lambda)$ (sunlight spectrum) and $\varepsilon(\lambda)$ (virus absorption) shown in Fig. 1, with $\Phi = 1.4 \times 10^{-2}$ mol Einstein^{-1} (Mattle et al., 2015) and $A_1(\lambda) = 0.45\ e^{-0.015\ \lambda}$ (Vione, 2020). The results of the relevant calculations are reported as solid squares in Fig. 2. The dashes curves represent data fit with Eq. (2), using η_{app} as the only free-floating variable after finding λ_{eq} = 307.5 nm.

On this basis, it was possible to fix p°(307.5 nm) = 4.04×10^{-12} Einstein cm^{-2} s^{-1} nm^{-1}, ε(307.5 nm) = 3.45×10^{5} M^{-1} cm^{-1}, and A_1(307.5 nm) = 0.00447 L $mg_C{}^{-1}$ cm^{-1}. With these parameter values, data fit returned η_{app} = 0.203 nm mol Einstein^{-1}. The excellent agreement between the k_{direct} data obtained with Eq. (1) and with Eq. (2) suggests that the EMW approximation can be applied well to the direct photoinactivation of phiX174.

It is not surprising to find λ_{eq} = 307.5 nm, when considering the absorption spectrum of phiX174, $\varepsilon(\lambda)$ (which is similar to that of many viral genomes) and the spectral photon flux density of sunlight, $p^{\circ}(\lambda)$ Fig. 1). The two spectra overlap in a rather narrow interval in the UVB region, and the product $p^{\circ}(\lambda)\ \varepsilon(\lambda)$ that appears in Eqs. (1),((2) shows a maximum that is quite near the value of λ_{eq}.

Considering that depth and DOC are the main water parameters

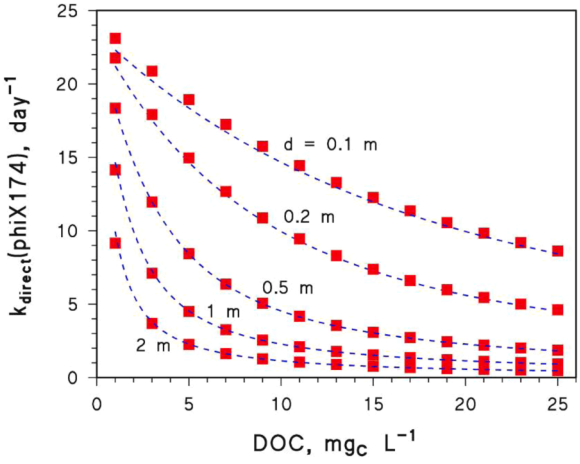

Fig. 2. Modeled first-order rate constants (k_{direct}) for the direct photoinactivation of the virus phiX174, for different values of water depth d and DOC (dissolved organic carbon). Depth and DOC values are referred to conditions in which photoinactivation is most effective (shallow waters) and has been studied in the field. Solid squares: data calculated by using Eq. (1). Dashes curves: fit results obtained by using Eq. (2) with η_{app} as fit variable.

affecting virus inactivation (Zhang et al., 2020), the variation ranges shown in Fig. 2 cover the majority of scenarios where solar inactivation can be taken advantage of in ponds and wetlands. The very good agreement between Eqs. (1) and (2) once the appropriate values of λ_{eq} and η_{app} are found suggests that the monochromatic approximation does not cause loss of generality in the photochemical model. The EMW approximation does not take into account the effects of vegetation and water body hydrology, but these effects are not considered in Eq. (1) as well. However, if they translate into a numerical factor, these can be easily included in both Eqs. (1) and (2).

3.2. Kinetic predictions as a function of latitude and the day of the year

3.2.1. Maximum (fair-weather) daily dose using the photon flux density of sunlight at solar noon: determination of F_1

The maximum daily dose $G_{day}^{max}(\lambda_{eq})$ was first calculated with Eq. (3), and the results of the calculations are shown as solid squares in Fig. 3. Then, these data were used for optimization with Eq. (4). The term F_1 in Eq. (4) was optimized for a latitude of 45 °N at λ_{eq} = 307.5 nm, and it took a value of 0.43 with a NRMSE of 1%. The value of F_1 thus obtained means that the average photon flux density of sunlight during the whole day length is 43 % of the photon flux density peak at the solar noon ($p_{sn}^{o}(\lambda_{eq})$, see Eq. (4)). The excellent data fit suggests that this value of F_1 (referred to fair-weather conditions at 45°N) is consistent during the year.

The next step consists in verifying if the value of F_1 depends on the latitude or if, in contrast, F_1 = 0.43 obtained at φ = 45 °N can be generalized. To do so, F_1 was validated with predictions of the cumulated radiation for latitudes from 60°S to 60°N, with a step of 5 °. The solid symbols reported in Fig. 4 represent the cumulated radiation G_{day}^{max}(307.5 nm), referred to the 15th day of each month and calculated by integration using Eq. (3). The curves represent the predictions obtained with Eq. (4), by using F_1 = 0.43. All the predictions showed a very good agreement with the Eq. (3) data, with errors of less than 13% for latitudes between 55 °S/55 °N, and 22–18% for 60 °S and 60 °N, respectively. This result means that a constant value F_1 = 0.43 can be used over the whole year in the whole latitude belt from 60 °S to 60 °N.

Replacing the term "$p^{o}(\lambda_{eq})\ \tau$" in Eq. (2) with the term "$F_1 \cdot p_{sn}^{o}(\lambda_{eq}) \cdot \tau_{DL}$" from Eq. (4) leads to the first-order rate constants for phiX174 direct photoinactivation in different months, for φ = 60°S-60°N. However, this approach only predicts virus photoinactivation kinetics in fair-weather conditions, which could overestimate the actual kinetics of inactivation by sunlight. Therefore, F_2 was added to account for the cloudiness and the effect on the irradiance that reaches the Earth's surface. The next section presents the validation of the Eq. (6) model against literature data.

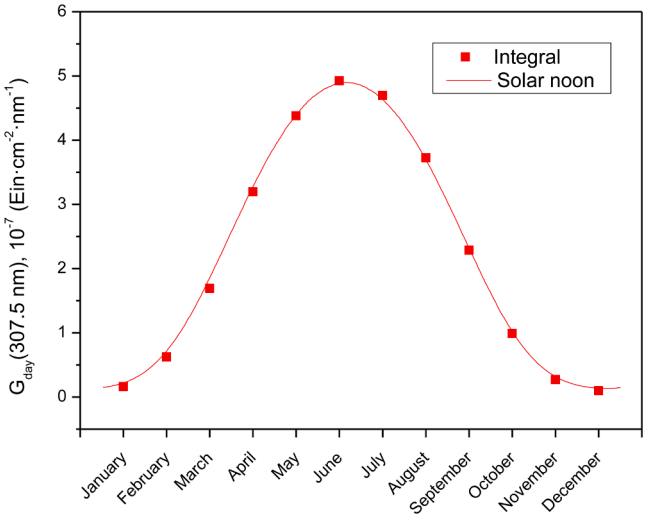

Fig. 3. Fit for the daily dose during the year for a latitude of 45°N. The solid squares represent the values calculated with Eq. (3) for the 15th day of each month. The solid line is the result of data optimization with Eq. (4), which gave F_1 = 0.43.

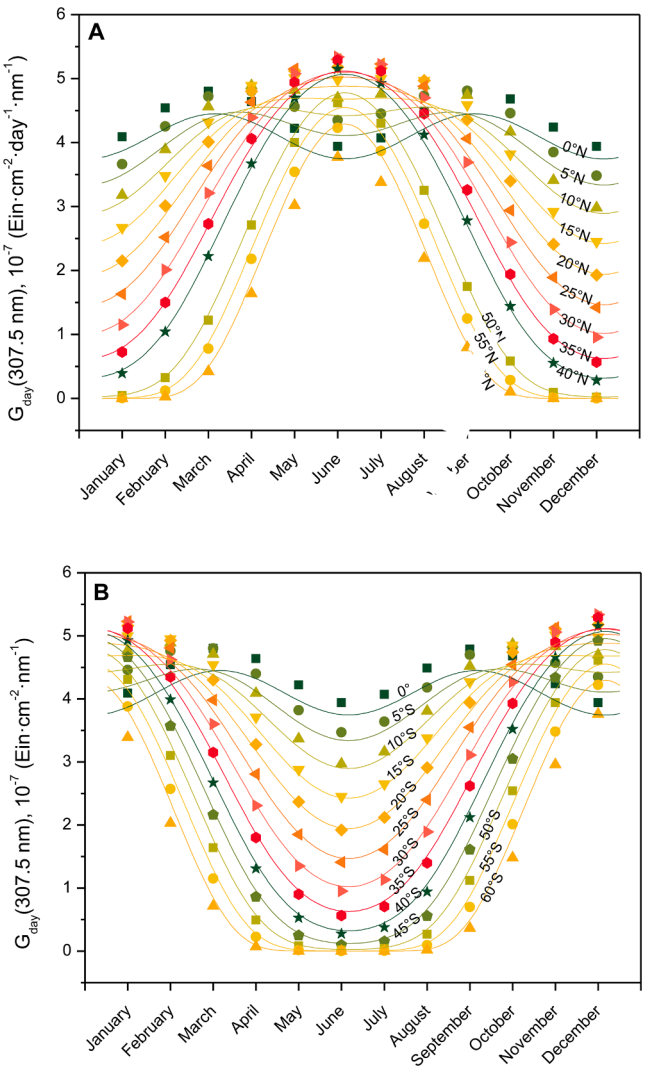

Fig. 4. Validation of the procedure to calculate the maximum cumulated incident radiation G_{day}^{max} (307.5 nm) as a function of the latitude and the day of the year, which suggests that F_1 = 0.43 works well on a global scale. A: Latitudes from 0 ° to 60 °N with steps of 5 ° (except 45°N that was used for optimization). B: Latitudes from 60 °S to 0 ° with steps of 5 °.

3.2.2. Realistic values of cumulated incident radiation: determination of F_2

The approximated Eq. (4) predicts well the maximum cumulated incident radiation (G_{day}^{max}(307.5 nm)) for varying latitude and season, but it does not include atmosphere or cloud-cover effects. In order to estimate a more realistic daily dose, the factor F_2 was calculated based on graphic data shown in Fig. 5 or the tabulated data in the F2.xlsx file provided as **SM**. To evaluate the accuracy of F_2, predictions for the cumulated incident radiation from 8.00 to 16.00 h at 52 °N latitude, calculated with Eq. (5) (obtained from Eq. (4) by multiplying for the F_2 factor) were compared to data from the literature (Frank and Klöpffer, 1988). In the cited paper, Frank and Klöpffer reported average radiation intensity referred to the time interval of solar noon ± 4 h. To obtain the measured cumulated incident radiation, these values were multiplied by Δt = 28,800 s (i.e., the time interval from 8.00 to 16.00 h). F_2 took a value of 0.58 (latitude 52 °, longitude 5 °). Similar values (57%) have

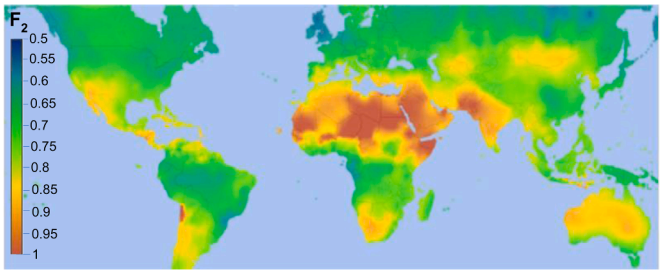

Fig. 5. Worldwide representation of the annual average values of F_2 calculated from historical data of the last 12 years, based on the procedure developed by Moreno-SanSegundo et al. (2021). This information is also available in the Excel file provided as **SM**.

been experimentally found at a latitude of 40.3 °N at Madrid, Spain (García-Gil et al., 2019).

Fig. 6 shows a good agreement between the predicted and literature data when using the estimated value of F_2 based on historical weather data, which reduces the NRMSE from 121% for $F_2 = 1$ to 25.5% for $F_2 = 0.58$. Therefore, an approach based on historical data of the weather considerably improves the prediction with respect to the assumption of fair-weather conditions.

3.3. Implications for the modeling of direct virus photoinactivation

Upon introduction of the new parameter F_2, Eq. (6) allows for the calculation of the kinetic constant for the direct photoinactivation of the virus phiX174. Moreover, considering that $G_{day}^{\max}(\lambda_{eq}) = F_1 \cdot p_{sn}^{o}(\lambda_{eq}) \cdot \tau_{DL}$ (Eq. (4)), a more compact form for the same equation becomes the following:

$$k_{direct} = \frac{10}{d} \cdot F_2 \cdot G_{day}^{\max}(\lambda_{eq}) \cdot \eta_{app} \cdot \frac{\varepsilon(\lambda_{eq})}{A_1(\lambda_{eq}) \cdot DOC} \left(1 - 10^{-100 \cdot A_1(\lambda_{eq}) \cdot d \cdot DOC}\right) \quad (7)$$

where $\lambda_{eq} = 307.5$ nm, $\eta_{app} = 0.203$ nm mol Einstein^{-1}, $\varepsilon(307.5\,\text{nm}) = 3.45 \times 10^5$ M^{-1} cm^{-1}, and $A_1(307.5\,\text{nm}) = 0.00447$ L mg$_C^{-1}$ cm^{-1}. The values of F_2 can be obtained from the latitude and longitude geocoordinates using Fig. 5 or the F2.xlsx file provided as **SM**. The calculated values for $G_{day}^{\max}$ (307.5 nm) are reported in Table 1 for latitudes between 60°S and 60°N with a step of 5 °, and for the 15th day of each month. Eq. (7) with these data allows for the calculation of k_{direct} for

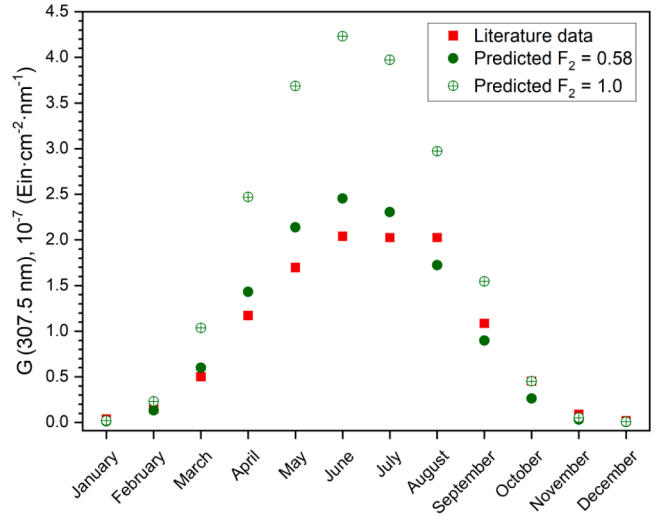

Fig. 6. Comparison between literature (red squares, Frank and Klöpffer, 1988) and predicted data (G_{day}^{real} (307.5 nm), circles) of the cumulated radiation intensity.

phiX174 at different latitudes and seasons, for different values of DOC and d. If additional data of $G_{day}^{\max}$ (307.5 nm) are needed for other latitudes (between 60 °S and 60 °N) or days, they can be calculated with Eq. (4) by considering that the values of photon flux density at solar noon, p_{sn}^{o}(307.5 nm), were obtained with Eq. (S6) as a function of month and latitude, while the values of τ_{DL} were obtained with Eq. (S7).

Eq. (7) takes into account all the main parameters that have been shown to affect the photoinactivation of viruses (irradiance, DOC, and water depth). Moreover, this equation also accounts for the effect of latitude and season on the first-order kinetic constant through the irradiance ($G_{day}^{\max}$). According to Eqs. (S1–S7), for latitudes close to the Equator, $G_{day}^{\max}$ remains almost constant, whereas for higher latitudes, τ_{DL} and p_{sn}^{o} increase in summer and decrease in winter (Fig. 4). The same trend applies to the first-order kinetic constant, which is directly proportional to $G_{day}^{\max}$. However, the value of F_2 cannot be predictively calculated based exclusively on the latitude and the day of the year, because it depends on the weather conditions. For example, for the Republic of Congo, a high value of the kinetic constant would be expected according to its location at the Equator. However, the high probability of cloud-cover based on historical weather data leads to a significantly lower expected kinetic constant in this region (Fig. 5).

The ultimate goal of the present study is to use the model thus obtained to predict virus inactivation in the field. To test the feasibility of this approach, predictions by Eq. (7) were compared with field data of photoinduced virus inactivation. The field results of Boehm et al. (2009) were taken into account that refer to the (presumably mostly direct, according to the authors) photoinactivation of somatic phages, with an overall behavior that has reasonable analogies with the direct photoinactivation of the somatic phage phiX174. The cited authors found a maximal photoinactivation rate of somatic phages of 28 day^{-1} I_{UVB}^{-1} in Avalon Bay, California (late August, 33 °N latitude, 0.15 m water depth, 7 mg$_C$ L^{-1} DOC). In order to compare this measurement with our model prediction, it was necessary to assess the value of I_{UVB}. That was obtained by using SMARTS (the same procedure used by the authors), giving an average value of 0.41 W m^{-2} that agrees with the published data (see Fig. 2 of Boehm. et al., 2009). By so doing, the field kinetic constant was calculated as 11.54 day^{-1}. F_2 took a value of 0.82 (latitude 33 °, longitude -118 °).

Our model prediction with Eq. (7) for phiX174 is $k_{direct} = 9.8$ day^{-1}. The error value of 15% looks more than reasonable if considering that the phages in the paper by Bohem et al. (2009) were not identical to those considered in our model, and that indirect photoinactivation by, most notably, $^1O_2$ could not be totally excluded (Bohem et al., 2009). Other differences between the model prediction and the field system include the high ionic strength and the presence of halide species in the marine environment. These factors have previously been found to enhance the photoinactivation of viruses (Sinton et al., 2002). Another possibility is the occurrence of consistent sunny weather during the field study, which took place during summer. For very bright and sunny regions the value of F_2 is around 90% (Moreno-SanSegundo et al., 2021) and, if Eq. (7) is recalculated with $F_2 = 0.9$ instead of $F_2 = 0.82$, $k_{direct} = 10.8$ day^{-1} is obtained that is not far from the field datum.

Note that a deactivation constant $k_{direct} \sim 11$ day^{-1} translates into a virus half-life time $t_{1/2} \sim 1.5$ h, as an average value from 8.00 h to 16.00 h. In the same 8 h time period, sunlight would thus be able to inactivate ~ 97.5% of the viruses that were initially present. Although this does not make complete disinfection, it would certainly help reduce the viral load in water.

4. Conclusions

- Here, we propose a relatively simple procedure to estimate the kinetic constant for the direct photoinactivation of the somatic phage phiX174, which is a typical model organism for the viruses that mainly undergo inactivation by the direct action of sunlight. The

Table 1
Predicted maximum cumulated incident radiation (G_{day}^{max} (307.5 nm)) as a function of latitude and month (data provided for the 15th day of each month). These values can be used in Eq. (7) to predict the rate constant k_{direct}.

	Predicted maximum cumulated incident radiation: G_{day}^{max} (307.5 nm) [Einstein $cm^{-2}nm^{-1}$]											
Latitude	January	February	March	April	May	June	July	August	September	October	November	December
60°S	3.82×10^{-7}	2.35×10^{-7}	9.36×10^{-8}	1.10×10^{-8}	1.20×10^{-10}	2.82×10^{-13}	6.14×10^{-12}	2.46×10^{-9}	4.81×10^{-8}	1.79×10^{-7}	3.39×10^{-7}	4.27×10^{-7}
55°S	4.16×10^{-7}	2.84×10^{-7}	1.39×10^{-7}	3.09×10^{-8}	2.31×10^{-9}	1.68×10^{-10}	5.78×10^{-10}	1.21×10^{-8}	8.54×10^{-8}	2.29×10^{-7}	3.79×10^{-7}	4.53×10^{-7}
50°S	4.45×10^{-7}	3.28×10^{-7}	1.88×10^{-7}	6.17×10^{-8}	1.15×10^{-8}	2.69×10^{-9}	5.19×10^{-9}	3.26×10^{-8}	1.29×10^{-7}	2.76×10^{-7}	4.13×10^{-7}	4.76×10^{-7}
45°S	4.68×10^{-7}	3.66×10^{-7}	2.35×10^{-7}	1.01×10^{-7}	3.12×10^{-8}	1.25×10^{-8}	1.87×10^{-8}	6.37×10^{-8}	1.76×10^{-7}	3.20×10^{-7}	4.41×10^{-7}	4.94×10^{-7}
40°S	4.85×10^{-7}	3.99×10^{-7}	2.80×10^{-7}	1.45×10^{-7}	6.17×10^{-8}	3.29×10^{-8}	4.32×10^{-8}	1.03×10^{-7}	2.23×10^{-7}	3.58×10^{-7}	4.62×10^{-7}	5.06×10^{-7}
35°S	4.95×10^{-7}	4.25×10^{-7}	3.21×10^{-7}	1.92×10^{-7}	1.00×10^{-7}	6.39×10^{-8}	7.76×10^{-8}	1.47×10^{-7}	2.68×10^{-7}	3.90×10^{-7}	4.77×10^{-7}	5.11×10^{-7}
30°S	4.98×10^{-7}	4.45×10^{-7}	3.57×10^{-7}	2.38×10^{-7}	1.45×10^{-7}	1.03×10^{-7}	1.19×10^{-7}	1.94×10^{-7}	3.10×10^{-7}	4.16×10^{-7}	4.85×10^{-7}	5.10×10^{-7}
25°S	4.95×10^{-7}	4.57×10^{-7}	3.88×10^{-7}	2.82×10^{-7}	1.92×10^{-7}	1.48×10^{-7}	1.65×10^{-7}	2.40×10^{-7}	3.47×10^{-7}	4.35×10^{-7}	4.86×10^{-7}	5.02×10^{-7}
20°S	4.85×10^{-7}	4.63×10^{-7}	4.12×10^{-7}	3.22×10^{-7}	2.39×10^{-7}	1.96×10^{-7}	2.13×10^{-7}	2.85×10^{-7}	3.78×10^{-7}	4.48×10^{-7}	4.81×10^{-7}	4.88×10^{-7}
15°S	4.69×10^{-7}	4.62×10^{-7}	4.29×10^{-7}	3.58×10^{-7}	2.84×10^{-7}	2.44×10^{-7}	2.60×10^{-7}	3.26×10^{-7}	4.04×10^{-7}	4.54×10^{-7}	4.69×10^{-7}	4.68×10^{-7}
10°S	4.47×10^{-7}	4.55×10^{-7}	4.41×10^{-7}	3.89×10^{-7}	3.27×10^{-7}	2.91×10^{-7}	3.06×10^{-7}	3.62×10^{-7}	4.24×10^{-7}	4.53×10^{-7}	4.51×10^{-7}	4.42×10^{-7}
5°S	4.20×10^{-7}	4.42×10^{-7}	4.46×10^{-7}	4.14×10^{-7}	3.66×10^{-7}	3.35×10^{-7}	3.48×10^{-7}	3.94×10^{-7}	4.37×10^{-7}	4.46×10^{-7}	4.27×10^{-7}	4.11×10^{-7}
0°	3.87×10^{-7}	4.22×10^{-7}	4.44×10^{-7}	4.34×10^{-7}	4.00×10^{-7}	3.75×10^{-7}	3.86×10^{-7}	4.20×10^{-7}	4.44×10^{-7}	4.33×10^{-7}	3.98×10^{-7}	3.75×10^{-7}
5°N	3.49×10^{-7}	3.96×10^{-7}	4.36×10^{-7}	4.47×10^{-7}	4.28×10^{-7}	4.11×10^{-7}	4.19×10^{-7}	4.41×10^{-7}	4.45×10^{-7}	4.13×10^{-7}	3.63×10^{-7}	3.35×10^{-7}
10°N	3.07×10^{-7}	3.65×10^{-7}	4.21×10^{-7}	4.53×10^{-7}	4.52×10^{-7}	4.43×10^{-7}	4.47×10^{-7}	4.55×10^{-7}	4.39×10^{-7}	3.88×10^{-7}	3.24×10^{-7}	2.90×10^{-7}
15°N	2.62×10^{-7}	3.29×10^{-7}	4.01×10^{-7}	4.53×10^{-7}	4.69×10^{-7}	4.68×10^{-7}	4.69×10^{-7}	4.63×10^{-7}	4.27×10^{-7}	3.57×10^{-7}	2.81×10^{-7}	2.43×10^{-7}
20°N	2.15×10^{-7}	2.89×10^{-7}	3.74×10^{-7}	4.47×10^{-7}	4.80×10^{-7}	4.88×10^{-7}	4.85×10^{-7}	4.65×10^{-7}	4.08×10^{-7}	3.21×10^{-7}	2.35×10^{-7}	1.95×10^{-7}
25°N	1.67×10^{-7}	2.45×10^{-7}	3.41×10^{-7}	4.34×10^{-7}	4.85×10^{-7}	5.02×10^{-7}	4.96×10^{-7}	4.60×10^{-7}	3.83×10^{-7}	2.80×10^{-7}	1.88×10^{-7}	1.47×10^{-7}
30°N	1.21×10^{-7}	1.98×10^{-7}	3.04×10^{-7}	4.14×10^{-7}	$4.83v10^{-7}$	5.09×10^{-7}	4.99×10^{-7}	4.48×10^{-7}	3.52×10^{-7}	2.36×10^{-7}	1.41×10^{-7}	1.03×10^{-7}
35°N	7.91×10^{-8}	1.52×10^{-7}	2.61×10^{-7}	3.88×10^{-7}	4.74×10^{-7}	5.11×10^{-7}	4.96×10^{-7}	4.30×10^{-7}	3.15×10^{-7}	1.90×10^{-7}	9.68×10^{-8}	6.32×10^{-8}
40°N	4.43×10^{-8}	1.07×10^{-7}	2.16×10^{-7}	3.55×10^{-7}	4.58×10^{-7}	5.05×10^{-7}	4.87×10^{-7}	4.04×10^{-7}	2.73×10^{-7}	1.43×10^{-7}	5.85×10^{-8}	3.23×10^{-8}
45°N	1.93×10^{-8}	6.70×10^{-8}	1.69×10^{-7}	3.17×10^{-7}	4.36×10^{-7}	4.94×10^{-7}	4.71×10^{-7}	3.72×10^{-7}	2.28×10^{-7}	9.87×10^{-8}	2.89×10^{-8}	1.21×10^{-8}
50°N	5.38×10^{-9}	3.49×10^{-8}	1.22×10^{-7}	2.73×10^{-7}	$4.07v10^{-7}$	4.76×10^{-7}	4.48×10^{-7}	3.34×10^{-7}	1.80×10^{-7}	5.97×10^{-8}	1.01×10^{-8}	2.49×10^{-9}
55°N	5.91×10^{-10}	1.33×10^{-8}	7.91×10^{-8}	2.25×10^{-7}	3.72×10^{-7}	4.52×10^{-7}	4.20×10^{-7}	2.91×10^{-7}	1.32×10^{-7}	2.93×10^{-8}	1.82×10^{-9}	1.34×10^{-10}
60°N	5.31×10^{-12}	2.83×10^{-9}	4.31×10^{-8}	1.75×10^{-7}	3.32×10^{-7}	4.26×10^{-7}	3.87×10^{-7}	2.43×10^{-7}	8.67×10^{-8}	1.01×10^{-8}	6.81×10^{-11}	9.60×10^{-14}

procedure is based on an approximated equation for monochromatic light absorption, which relies on the identification of the equivalent monochromatic wavelength that best simulates the behavior of the polychromatic system.

- The main advantage of this approach is to obtain a simple and manageable equation (Eq. (7)) to easily predict inactivation kinetics, with no need to use external and complex software. Predictions were quite good in the case of somatic phages undergoing direct photoinactivation in the field. To extend the model to other types of viruses, the corresponding values of Φ and $\varepsilon(\lambda)$ are required.
- The simplicity of the procedure leads to a few limitations that do not really compromise its usefulness. For example, for latitudes in which there is no sunrise or sunset in some seasons, this procedure is not applicable because τ_{DL} cannot be calculated with Eq. (S7). However, in these latitudes (below 60°S and above 60°N), the incident radiation received is not enough to take advantage of a sunlight-mediated process. The most significant limitation is probably the fact that considering average weather with the F_2 parameter would not fit well periods with consistently fine or bad weather. However, this is a handicap that more complex, software-based polychromatic approaches would not solve either.

Declaration of Competing Interest

The authors declare that they have no known competing financial interests or personal relationships that could have appeared to influence the work reported in this paper.

Acknowledgments

Ángela García Gil acknowledges Spanish Ministry of Education for her FPU grant (FPU17/04333). The authors gratefully acknowledge the financial support of European Union's Horizon 2020 research and innovation programme in the frame of the PANIWATER project (GA 820718), funded under the Indo-EU International Water cooperation sponsored jointly by European Commission and Department of Science and Technology, India.

Supplementary materials

Supplementary material associated with this article can be found, in the online version, at doi:10.1016/j.watres.2021.117837.

References

Boehm, A.B., Yamahara, K.M., Love, D.C., Peterson, B.M., Mcneill, K., Nelson, K.L., 2009. Covariation and photoinactivation of traditional and novel indicator organisms and human viruses at a sewage-impacted marine beach. Environ. Sci. Technol. 43, 8046–8052.

Carratalà, A., Calado, A.D., Mattle, M.J., Meierhofer, R., Luzi, S., Kohn, T., 2016. Solar disinfection of viruses in polyethylene terephthalate bottles. Appl. Environ. Microbiol. 82, 279–288.

Curtis, T.P., Mara, D.D., Dixo, N.G.H., Silva, S.A., 1994. Light penetration in waste stabilization ponds. Water Res. 28, 1030–1038.

Dias, D.F.C., Passos, R.G., von Sperling, M., 2017. A review of bacterial indicator disinfection mechanisms in waste stabilisation ponds. Rev. Environ. Sci. Biotechnol. 16, 517–539.

Fisher, M.B., Love, D.C., Schuech, R., Nelson, K.L., 2011. Simulated sunlight action spectra for inactivation of MS2 and PRD1 bacteriophages in clear water. Environ. Sci. Technol. 45, 9249–9255.

Frank, R., Klöpffer, W., 1988. Spectral solar photo irradiance in central europe and the adjacent north Sea. Chemosphere 17, 985–994.

García-Gil, Á., Casado, C., Pablos, C., Marugán, J., 2019. Novel procedure for the numerical simulation of solar water disinfection processes in flow reactors. Chem. Eng. J. 376, 120194.

García-Gil, Á., Martínez, A., Polo-López, M.I., Marugán, J., 2020a. Kinetic modeling of the synergistic thermal and spectral actions on the inactivation of viruses in water by sunlight. Water Res. 183, 116074.

García-Gil, Á., Abeledo-Lameiro, M.J., Gómez-Couso, H., Marugán, J., 2020b. Kinetic modeling of the synergistic thermal and spectral actions on the inactivation of cryptosporidium parvum in water by sunlight. Water Res. 185, 116226.

Giannakis, S., Ruales-Lonfat, C., Rtimi, S., Thabet, S., Cotton, P., Pulgarin, C., 2016. Castles fall from inside: evidence for dominant internal photo-catalytic mechanisms during treatment of saccharomyces cerevisiae by photo-fenton at near-neutral pH. Appl. Catal. B Environ. 185, 150–162.

Giannakis, S., Voumard, M., Rtimi, S., Pulgarin, C., 2018. Bacterial disinfection by the photo-fenton process: extracellular oxidation or intracellular photo-catalysis? Appl. Catal. B Environ. 227, 285–295.

Kalogirou, S.A., 2013. Chapter 2 - environmental characteristics. View on ScienceDirect Solar Energy Engineering. Academic Press, pp. 51–123. ISBN 9780123972569.

Kohn, T., Nelson, K.L., 2007. Sunlight-mediated inactivation of MS2 coliphage via exogenous singlet oxygen produced by sensitizers in natural waters. Environ. Sci. Technol. 41, 192–197.

Kohn, T., Grandbois, M., McNeill, K., Nelson, K.L., 2007. Association with natural organic matter enhances the sunlight-mediated inactivation of MS2 coliphage by singlet oxygen. Environ. Sci. Technol. 41, 4626–4632.

Kohn, T., Mattle, M.J., Minella, M., Vione, D., 2016. A modeling approach to estimate the solar disinfection of viral indicator organisms in waste stabilization ponds and surface waters. Water Res. 88, 912–922.

Love, D.C., Silverman, A., Nelson, K.L., 2010. Human virus and bacteriophage inactivation in clear water by simulated sunlight compared to bacteriophage inactivation at a Southern California beach. Environ. Sci. Technol. 44, 6965–6970.

Maiga, Y., Wethe, J., Denyigba, K., Ouattara, A.S., 2009. The impact of pond depth and environmental conditions on sunlight inactivation of Escherichia Coli and enterococci in wastewater in a warm climate. Can. J. Microbiol. 55, 1364–1374.

Maraccini, P.A., Wenk, J., Boehm, A.B., 2016. Exogenous indirect photoinactivation of bacterial pathogens and indicators in water with natural and synthetic photosensitizers in simulated sunlight with reduced UVB. J. Appl. Microbiol. 121, 587–597.

Mattle, M.J., Vione, D., Kohn, T., 2015. Conceptual model and experimental framework to determine the contributions of direct and indirect photoreactions to the solar disinfection of MS2, phiX174, and adenovirus. Environ. Sci. Technol. 49, 334–342.

McGuigan, K.G., Conroy, R.M., Mosler, H.J., du Preez, M., Ubomba-Jaswa, E., Fernandez-Ibañez, P., 2012. Solar water disinfection (SODIS): a review from bench-top to roof-top. J. Hazard. Mater. 235–236, 29–46.

Mc Neill, K., Canonica, S., 2016. Triplet state dissolved organic matter in aquatic photochemistry: reaction mechanisms, substrate scope, and photophysical properties. Environ. Sci. Processes Impacts 18, 1381–1399.

Moreno-SanSegundo, J., Giannakis, S., Samoili, S., Farinelli, G., McGuigan, K.G., Marugán, J., 2021. SODIS potential: a novel parameter to assess the suitability of solar water disinfection worldwide. Chem.. Eng. J. 419, 129889.

Nelson, K.L., Boehm, A.B., Davies-Colley, R.J., Dodd, M.C., Kohn, T., Linden, K.G., Liu, Y., Maraccini, P.A., McNeill, K., Mitch, W.A., et al., 2018. Sunlight-mediated inactivation of health-relevant microorganisms in water: a review of mechanisms and modeling approaches. Environ. Sci. Process Impacts 20, 1089–1122.

Nguyen, M.T., Silverman, A.I., Nelson, K.L., 2014. Sunlight inactivation of MS2 coliphage in the absence of photosensitizers: Modeling the endogenous inactivation rate using a photoaction spectrum. Environ. Sci. Technol. 48, 3891–3898.

NREL, 2021. National renewable energy laboratory, solar position algorithm NREL. Available online: https://midcdmz.nrel.gov/solpos/spa.html (accessed on Jun 27, 2021).

Romero, O.C., Straub, A.P., Kohn, T., Nguyen, T.H., 2011. Role of temperature and Suwannee River natural organic matter on inactivation kinetics of rotavirus and bacteriophage MS2 by solar irradiation. Environ. Sci. Technol. 45, 10385–10393.

Rosado-Lausell, S.L., Wang, H., Gutiérrez, L., Romero-Maraccini, O.C., Niu, X.Z., Gin, K. Y.H., Croué, J.P., Nguyen, T.H., 2013. Roles of singlet oxygen and triplet excited state of dissolved organic matter formed by different organic matters in bacteriophage MS2 inactivation. Water Res. 47, 4869–4879.

Rosario-Ortiz, F.L., Canonica, S., 2016. Probe compounds to assess the photochemical activity of dissolved organic matter. Environ. Sci. Technol. 50, 12532–12547.

Serna-Galvis, E.A., Troyon, J.A., Giannakis, S., Torres-Palma, R.A., Minero, C., Vione, D., Pulgarin, C., 2018. Photoinduced disinfection in sunlit natural waters : Measurement of the second order inactivation rate constants between E . coli and photogenerated transient species. Water Res. 147, 242–253.

Serna-Galvis, E.A., Troyon, J.A., Giannakis, S., Torres-Palma, R.A., Carena, L., Vione, D., Pulgarin, C., 2019. Kinetic modeling of lag times during photo-induced inactivation of E. coli in sunlit surface waters: unraveling the pathways of exogenous action. Water Res. 163, 114894.

Silverman, A.I., Nguyen, M.T., Jasper, J.T., Boehm, A.B., Nelson, K.L., 2015. Sunlight inactivation of fecal indicator bacteria in open-water unit process treatment wetlands: Modeling endogenous and exogenous inactivation rates. Environ. Sci. Technol. 49, 2757–2766.

Silverman, A.I., Tay, N., Machairas, N., 2019. Comparison of biological weighting functions used to mdel edogenous snlight iactivation rtes of MS2 cliphage. Water Res. 151, 439–446.

Sinton, L.W., Hall, C.H., Lynch, P.A., Davies-Colley, R.J., 2002. Sunlight inactivation of fecal indicator bacteria and bacteriophages from waste stabilization pond effluent in fresh and saline waters. Appl. Environ. Microbiol. 68, 1122–1131.

Vione, D., Minella, M., Maurino, V., Minero, C., 2014. Indirect photochemistry in sunlit surface waters: photoinduced production of reactive transient species. Chem. Eur. J. 20, 10590–10606.

Vione, D., 2020. A critical view of the application of the APEX software (aqueous photochemistry of environmentally-occurring xenobiotics) to predict photoreaction kinetics in surface freshwaters. Molecules 25 article n. 9.
Vione, D., 2021. The modelling of surface-water photoreactions made easier: introducing the concept of 'equivalent monochromatic wavelengths. Water Res. 190, 116675.
Zhang, X., Lardizabal, A., Silverman, A.I., Vione, D., Kohn, T., Nguyen, T.H., Guest, J.S., 2020. Global Sensitivity Analysis of Environmental, Water Quality, Photoreactivity, and Engineering Design Parameters in Sunlight Inactivation of Viruses. Environ. Sci. Technol. 54, 8401–8410.